

# A phenomenological study on the production of Higgs bosons in the cSMCS model at the LHC

*N. Darvishi<sup>a\*</sup> and M.R. Masouminia<sup>b†</sup>*

<sup>a</sup> *Faculty of Physics, University of Warsaw, Pasteura 5, 02-093 Warsaw, Poland*

<sup>b</sup> *Department of Physics, University of Tehran, 1439955961, Tehran, Iran*

In the present work, we intend to predict the production rates of the Higgs bosons in the simplest extension of the Standard Model (SM) by a neutral complex singlet (cSMCS). This model has an additional source of CP violation and provides strong enough first-order electroweak phase transition to generate the baryon asymmetry of universe (BAU). The scalar spectrum of the cSMCS includes three neutral Higgs particles with the lightest one considered to be the 125 GeV Higgs boson found at LHC. The SM-like Higgs boson comes mostly from the SM-like SU(2) doublet, with a small correction from the singlet. To predict the production rates of the Higgs bosons, we use a conventional effective LO QCD framework and the unintegrated parton distribution functions (UPDF) of Kimber-Martin-Ryskin (KMR). We first compute the SM Higgs production cross-section and compare the results to the existing theoretical calculations from different frameworks as well as the experimental data from the CMS and ATLAS collaborations. It is shown that our framework is capable of producing sound predictions for these high-energy QCD events in the SM. Afterwards we present our predictions for the Higgs boson production in the cSMCS.

## I. INTRODUCTION

In order to achieve a better understanding of the fundamental interactions, it is instructive to produce accurate and reliable predictions for the observables that can be measured in the ongoing experimental efforts. The Standard Model (SM) has been particularly successful in producing valuable and surprisingly accurate predictions. The experimental confirmation of these predictions provoked inspiration to search for new phenomena. However, the SM is not a complete and perfect model, in that it is unable to provide adequate explanations for many questions in particle and astrophysics. One way of addressing these problems is to enlarge the SM with an extended scalar sector. Here we focus on one of the simplest extension of SM by a complex Singlet (cSMCS) [1–3]. Such choice for the extension sector have been widely discussed in the literature, see for example the references [4–13]. The cSMCS has an additional source of spontaneous CP violation and provides strong enough first-order electroweak phase transition to generate baryon asymmetry of universe (BAU). Also in the reference [1], it has been argued that to predict an acceptable value for the BAU, the SMCS should be accompanied with heavy vector quarks (they are not included here). Considering a softly broken global U(1) symmetry with the potential of the SMCS model, leads to the so-called constraint SMCS (cSMCS) model. The model that has been considered here is a part of a larger framework, presented in [14], where the extension of the SM by an inert doublet (with  $vev = 0$ ) and a complex singlet (cIDMS) has been studied, focusing the properties of dark matter. This model that we consider contains

three neutral Higgs particles. We have considered the lightest one to be the 125 GeV Higgs boson found at the LHC. The SM-like Higgs boson comes mostly from the SM-like SU(2) doublet, with a small correction from the singlet. The cSMCS contains two additional Higgs scalars,  $h_i$ ,  $i = 2, 3$  and  $m_{h_i} > m_{h_1} \simeq 125$  GeV, which are taken to be

$$m_{h_3} \gtrsim m_{h_2} > 150 \text{ GeV}. \quad (1)$$

We test the predictions of the SM by collecting precise measurements of observables possibly sensitive to new physics, an example being the campaign to determine the Higgs couplings to other SM particles. Then we search of the effects from new particles in colliders, by performing a complete set of high-energy QCD investigations over the lesser known physical territory that is being described by the sSMCS.

It is well-known that the main contribution into the hadronic cross-section of the production of the Higgs bosons at the LHC,

$$P_1 + P_2 \rightarrow H + X,$$

is the so-called gluon-gluon fusion sub-process, i.e.

$$g^*(k_1) + g^*(k_2) \rightarrow H(p), \quad (2)$$

via a single triangular top-quark loop, see the figure 1 part (a). Also, the Higgs boson production accompanied with a single jet or double jets can be traced back to the quark-box loops (figure 1 part (b)) and the quark-pentagon loops (figure 1 part (c)), respectively. These are, by all means, some higher order corrections to the triangular top-quark loop diagram. Other involving processes (the  $t\bar{t}$ -fusion sub-process, figure 1 part (c), and the  $W/Z$  Bremsstrahlung sub-processes, figure 1 parts (e) and (f), are expected to produce roughly one tenth of the production rate at the present LHC energies, [15]).

\* neda.darvishi@fuw.edu.pl

† m.masouminia@ut.ac.ir

Please note that in principle, one have to include the contributions of all quark flavors in such diagrams. However, limiting our calculations to the top-quark loops can be justified, knowing that the SM Higgs boson coupling to the top quark is considerably (nearly 35 times) stronger compared to the bottom quark. This leads to a relative suppression of other quark contributions about 1200 or more. Additionally, in order to have a complete understanding over the dynamics of such processes, one have to account for all of the relevant processes and their higher-order corrections. Nevertheless, it has been shown that one can replace such complicated calculation by using a higher-order correction factor (i.e. the K-factor, [15], also see the section IV). Throughout the years numerous theoretical and phenomenological attempts have been made, trying to explore different aspects and dynamics of the production of the Higgs particles at the LHC, within the SM, e.g. the references [15–23].

Such calculations are conventionally carried out in the collinear approximation, where the contributing processes are quite complicated even at the lowest order, given the complexity of evaluating the matrix elements of the quark-loops. However, it is customary to introduce the "large top-quark mass" approximation, simplifying the processes (up to one loop) through implementing an effective vertex instead of the loop. Using this large  $m_t$  approximation, the total cross-section of the production of the Higgs boson via the  $g^* + g^* \rightarrow H$  sub-process have been calculated up to the next-to-next-to-leading order (NNLO) QCD accuracy, [18, 21].

In the collinear factorization framework, the total cross-section of the production of a Higgs boson can be written as the partonic cross-section of the involving sub-process ( $\hat{\sigma}_{gg \rightarrow H}$ ), times the probability of appearing that particular partonic configuration at top of the evolution ladder of the individual hadrons, i.e.,

$$\sigma_{P+P \rightarrow H+X} = \int_0^1 \frac{dx_1}{x_1} \int_0^1 \frac{dx_2}{x_2} x_1 g(x_1, \mu_1^2) x_2 g(x_2, \mu_2^2) \times \hat{\sigma}_{gg \rightarrow H}(x_1, k_{1,t}^2 = 0, \mu_1^2; x_2, k_{2,t}^2 = 0, \mu_2^2) (3)$$

$g(x_i, \mu_i^2)$ , the single-scaled (gluonic) parton distribution functions (PDF), are the solutions of the Dokshitzer-Gribov-Lipatov-Altarelli-Parisi (DGLAP) evolution equations, [24–27]. These functions parametrize the probability of finding a gluon, emitting from the  $i$ th hadron and carrying the fraction  $x_i$  of its longitudinal momentum.  $\mu$  is an ultra-violet cutoff, related to the virtuality of the exchanged gluon during the inelastic scattering and  $k_{i,t}$  are the (neglected) transverse momenta of the incoming gluons. Omitting the transverse momentum contributions of the incoming partons can seriously lower the precision of the calculations, predominantly in the high center-of-mass events and in the small- $x$  regions, [15, 28–31]. Knowing this have brought up the necessity of introducing some transverse momentum dependent prton distribution functions (TMD PDF), notably the Ciafaloni-Catani-Fiorani-Marchesini

(CCFM) evolution equation [32–36], the Balitski-Fadin-Kuraev-Lipatov (BFKL) evolution equation, [37–41], and the unintegrated parton distribution functions (UPDF) of the  $k_t$ -factorization, namely the leading order (LO) Kimber-Martin-Ryskin (KMR) and LO and next-to-leading order (NLO) Martin-Ryskin-Watt (MRW) formalisms, [28, 29]. Recently, it has been shown that these UPDF, specially in the KMR formalism, are very effective in providing successful theoretical descriptions of the existing experimental data, [42–46].

In the present work, we calculate the total cross-section of the production of the Higgs bosons beyond the SM for predicting the observable features of the extra scalar particles that are proposed within the cSMCS. By this end, we will demonstrate that our framework is capable of producing acceptable predictions for the know SM Higgs boson. To do this, we have calculated the inclusive total cross-section of the production of this particle and compared the results with the existing predictions from other theoretical frameworks as well as the experimental data from the CMS and the ATLAS collaborations, the references [47–49]. Afterwards, we present our analysis for the extra Higgs particles, going through the benchmarks of the cSMCS (see the section II) which are in agreement with the latest measurements of the precise electroweak (EW) data tests (i.e. the  $S$  and  $T$  parameters) and the signal strength,  $\mathcal{R}_{\gamma\gamma}$ . We hope that this work will provide some insight to the physics of the high-energy QCD events in a realm, beyond the SM.

The outlook of this paper is as follows: In the section II we present a brief introduction to the general structure of the cSMCS, including its scalar spectrum, its modifications and improvements over the SM. Section III contains a comprehensive description over the utilities and the means for the calculation of the cross-section of the Higgs bosons in hadron-hadron collisions, particularly targeting the events that take place at the LHC. The necessary numerical analysis will be presented in section IV, after which a thoroughgoing conclusion will follow in the section the V.

## II. THE CSMCS: THE SM PLUS A COMPLEX SINGLET SCALAR

The full Lagrangian of this model is given by

$$\mathcal{L} = \mathcal{L}_{gf}^{SM} + \mathcal{L}_{scalar} + \mathcal{L}_Y(\psi_f, \Phi), \quad (4)$$

the first term  $\mathcal{L}_{gf}^{SM}$  describes the interaction between SM gauge boson ( $W^\pm, Z$ )- SM fermion,  $\mathcal{L}_{scalar}$  describes the scalar sector of the model with one SU(2) doublet  $\Phi$  and a neutral complex scalar (spinless) singlet  $\chi$ .  $\mathcal{L}_Y(\psi_f, \Phi)$  represents, the Yukawa interaction of  $\Phi$  with SM fermions. Within our model the neutral complex singlet  $\chi$  does not couple to the SM fermions and gauge bosons. The singlet- SM fermion interactions present through the mixing of the singlet  $\chi$  with the doublet

$\Phi$  (it is same for the singlet interaction with the gauge bosons). We assume  $\Phi$  and  $\chi$  fields have non-zero vacuum expectation values ( $vev$ )  $v$  and  $we^{i\xi}$ , respectively ( $v, w, \xi \in \mathbf{R}$ ). The following field decomposition around the vacuum state are used,

$$\Phi = \begin{pmatrix} \phi^+ \\ \frac{1}{\sqrt{2}}(v + \phi_1 + i\phi_4) \end{pmatrix}, \chi = \frac{1}{\sqrt{2}}(we^{i\xi} + \phi_2 + i\phi_3), \quad (5)$$

through this work, we use  $w_1 = w \cos \xi$  and  $w_2 = w \sin \xi$  definitions. Masses of the gauge bosons are given by the  $vev$  of the doublet as in the SM, e.g  $M_W^2 = g^2 v^2/4$  for the  $W$  boson.

### A. Potential

The scalar potential of the model can be written as follows [1–3, 14]

$$V = V_D + V_S + V_{DS}, \quad (6)$$

$V_D$  and  $V_S$  are respectively the pure doublet and the pure singlet parts. The SM part of the potential represent by  $V_D$ , is equal to

$$V_D = -\frac{1}{2}m_{11}^2\Phi^\dagger\Phi + \frac{1}{2}\lambda(\Phi^\dagger\Phi)^2. \quad (7)$$

The potential for a complex singlet  $V_S$  is equal to,

$$\begin{aligned} V_S = & -\frac{1}{2}m_4^2(\chi^{*2} + \chi^2) - \frac{1}{2}m_s^2\chi^*\chi + \lambda_{s1}(\chi^*\chi)^2 \\ & + \lambda_{s2}(\chi^*\chi)(\chi^2 + \chi^{*2}) + \lambda_{s3}(\chi^4 + \chi^{*4}) \\ & + \kappa_1(\chi + \chi^*) + \kappa_2(\chi^3 + \chi^{*3}) + \kappa_3(\chi + \chi^*)(\chi^*\chi). \end{aligned} \quad (8)$$

The doublet-singlet interaction terms are:

$$\begin{aligned} V_{DS} = & \Lambda_1(\Phi^\dagger\Phi)(\chi^*\chi) + \Lambda_2(\Phi^\dagger\Phi)(\chi^2 + \chi^{*2}) \\ & + \kappa_4(\Phi^\dagger\Phi)(\chi + \chi^*). \end{aligned} \quad (9)$$

There are three quadratic terms ( $m_i^2$ ), six dimensionless quartic ( $\lambda_i, \Lambda_i$ ) and four dimensionful parameters  $\kappa_i$ ,  $i = 1, 2, 3, 4$ , describing linear ( $\kappa_1$ ) and cubic terms ( $\kappa_2, \kappa_3$ ) and  $\kappa_4$ . The linear term  $\kappa_1$  can be removed by a translation of the singlet field. The potential is symmetry under the  $\chi \rightarrow \chi^*$  transformation. We impose a global  $U(1)$  symmetry to reduce the number of parameters in the potential [1–3, 14].

$$U(1) : \Phi \rightarrow \Phi, \chi \rightarrow e^{i\alpha}\chi. \quad (10)$$

However, a non-zero  $vev$  of singlet would lead to a case spontaneous breaking of this symmetry and an appearance of massless Nambu-Goldstone scalar particles, what is not acceptable. To solve this, we shall consider a potential with a soft-breaking of  $U(1)$  symmetry terms, means the singlet cubic terms  $\kappa_{2,3}$ ,  $\kappa_4$  and the singlet quadratic term  $m_4^2$  are kept. Therefore, the potential remain with

the  $U(1)$ -symmetric terms ( $m_{11}^2, m_s^2, \lambda, \lambda_{s1}, \Lambda_1$ ) and the  $U(1)$ -soft-breaking terms ( $m_4^2, \kappa_{2,3,4}$ ) as follows, We will use the following notation for simplicity:  $\lambda_s = \lambda_{s1}, \Lambda = \Lambda_1$ ,

$$\begin{aligned} V = & -\frac{1}{2}m_{11}^2\Phi^\dagger\Phi + \frac{1}{2}\lambda(\Phi^\dagger\Phi)^2 + \Lambda(\Phi^\dagger\Phi)(\chi^*\chi) \\ & -\frac{1}{2}m_4^2(\chi^2 + \chi^{*2}) - \frac{1}{2}m_s^2\chi^*\chi + \lambda_s(\chi^*\chi)^2 \\ & + \kappa_2(\chi^3 + \chi^{*3}) + \kappa_3(\chi + \chi^*)(\chi^*\chi) + \kappa_4(\Phi^\dagger\Phi)(\chi + \chi^*). \end{aligned} \quad (11)$$

All the parameters of the potential are real.  $V$  is symmetry under the  $\chi \rightarrow \chi^*$  transformation and is explicitly CP conserving. We shall call the model with this choice of parameters, cSMCS [1–3].

### B. Physical states in the Higgs sector

The mass matrix  $M_{mix}^2$  that describes the singlet-doublet mixing, in the basis of neutral fields  $\phi_1, \phi_2, \phi_3$  is as follows:

$$M_{mix}^2 = \begin{pmatrix} M_{11} & M_{12} & M_{13} \\ M_{21} & M_{22} & M_{23} \\ M_{31} & M_{32} & M_{33} \end{pmatrix}, \quad (12)$$

where the  $M_{ij}(i, j = 1, 2, 3)$  are:

$$\begin{aligned} M_{11} &= v^2\lambda_1, \\ M_{12} &= v(w_1\Lambda + \sqrt{2}\kappa_4), \\ M_{13} &= vw_2\Lambda, \\ M_{22} &= \frac{w^2}{\sqrt{2}w_1} (3\kappa_2 + \kappa_3(1 + 2(w_1^2 - w_2^2)/w^2) \\ & \quad - \kappa_4v^2/w^2) + 2w_1^2\lambda_s, \\ M_{23} &= w_2(2w_1\lambda_s + \sqrt{2}(-3\kappa_2 + \kappa_3)), \\ M_{33} &= 2w_2^2\lambda_s. \end{aligned} \quad (13)$$

Diagonalization of  $M_{mix}^2$  (12) gives the mass-eigenstates  $h_1, h_2$  and  $h_3$ ,

$$\begin{pmatrix} h_1 \\ h_2 \\ h_3 \end{pmatrix} = R \begin{pmatrix} \phi_1 \\ \phi_2 \\ \phi_3 \end{pmatrix}, \quad RM_{mix}^2R^T = \text{diag}(m_{h_1}^2, m_{h_2}^2, m_{h_3}^2), \quad (14)$$

where

$$R = \begin{pmatrix} c_1c_2 & c_3s_1 - c_1s_2s_3 & c_1c_3s_2 + s_1s_3 \\ -c_2s_1 & c_1c_3 + s_1s_2s_3 & -c_3s_1s_2 + c_1s_3 \\ -s_2 & -c_2s_3 & c_2c_3 \end{pmatrix}. \quad (15)$$

All  $\alpha_i$  vary over an interval of length  $\pi$ . The full rotation matrix  $R$  depends on the mixing of  $\alpha_1, \alpha_2$  and  $\alpha_3$  angles and  $c_i = \cos \alpha_i$  and  $s_i = \sin \alpha_i$ . An important relations can be derived from the equations (14) and (15), i.e,

$$\phi_1 = c_1c_2h_1 - c_2s_1h_2 - s_2h_3, \quad (16)$$

with  $R_{11} = c_1 c_2$ ,  $R_{21} = c_2 s_1$  and  $R_{31} = s_2$ . The Yukawa interactions between the Higgs fields and the fermions ( $\mathcal{L}_Y$ ) generates the fermion masses. Note that only the doublet couples to the fermions.

$$\mathcal{L}_Y = - \sum_f \frac{m_f}{v} \bar{f} f (R_{11} h_1 + R_{21} h_2 + R_{31} h_3) \quad (17)$$

The table I presents the benchmarks of the cSMCS model, A1 through A7 obtained in reference [2], where the coupling and the masses are given. These are acquired by scanning the parameter space of the model. It can be seen in the table I that  $h_1$  is the SM-like Higgs boson. To see a complete discussion regarding this procedure, see the reference [2].

In the next section, we will introduce the necessary theoretical framework for the computation of the SM and cSMCS production rates in the high-energy QCD hadron-hadron collisions.

### III. CALCULATION OF THE HIGGS PRODUCTION CROSS-SECTION

Correctly assuming that the gluons entering the  $g^* + g^* \rightarrow H$  sub-process have some non-negligible transverse momenta, one is forced to include this contribution into the total cross-section of Higgs production using the defining identity of the  $k_t$ -factorization, [50],

$$a(x, \mu^2) = \int^{\mu^2} \frac{dk_t^2}{k_t^2} f_a(x, k_t^2, \mu^2), \quad (18)$$

where  $a(x, \mu^2)$  represents the solutions of the DGLAP evolution equations for both quarks and gluons, i.e.  $xq(x, \mu^2)$  and  $xg(x, \mu^2)$  respectively.  $f_a(x, k_t^2, \mu^2)$  are the UPDF of the  $k_t$ -factorization (the reader can find a comprehensive description over the structure and the kinematics of these UPDF in the reference [28, 29, 44]). Thus the equation (3) can be rewritten as follows:

$$\begin{aligned} \sigma_{P+P \rightarrow H+X} = & \int_0^1 \frac{dx_1}{x_1} \int_0^1 \frac{dx_2}{x_2} \int_0^\infty \frac{dk_{1,t}^2}{k_{1,t}^2} \int_0^\infty \frac{dk_{2,t}^2}{k_{2,t}^2} \\ & \times f_g(x_1, k_{1,t}^2, \mu_1^2) f_g(x_2, k_{2,t}^2, \mu_2^2) \\ & \times \hat{\sigma}_{gg \rightarrow H}(x_1, k_{1,t}^2, \mu_1^2; x_2, k_{2,t}^2, \mu_2^2). \end{aligned} \quad (19)$$

The contributing partonic cross-section,  $\hat{\sigma}_{gg \rightarrow H}$ , is conventionally defined as

$$d\hat{\sigma}_{gg \rightarrow H} = \frac{d\phi_{gg \rightarrow H}}{F_{gg \rightarrow H}} |\mathcal{M}(g^*(k_1) + g^*(k_2) \rightarrow H(p))|^2, \quad (20)$$

where  $k_i$  and  $p$  respectively represent the 4-momenta of the incoming gluons and the produced Higgs boson.  $d\phi_{gg \rightarrow H}$  and  $F_{gg \rightarrow H}$  are the corresponding particle phase space and the flux factor,

$$d\phi_{gg \rightarrow H} = \frac{d^3 p}{2E} \delta^{(4)}(k_1 + k_2 - p), \quad (21)$$

$$F_{gg \rightarrow H} = x_1 x_2 s, \quad (22)$$

with  $s$  being the center of mass energy squared,

$$s = (p_1 + p_2)^2 = 2p_1 \cdot p_2,$$

in the infinite momentum frame, i.e. where one can safely neglect the masses of the incoming hadrons in comparison with their incoming momenta ( $p_i \gg m_i$ ). Additionally,  $d\phi_{gg \rightarrow H}$  can be characterized in terms of the transverse momenta of the produced Higgs boson,  $p_t$ , its rapidity,  $y_H$ , and the azimuthal angles of its emission,  $\varphi$ ,

$$\frac{d^3 p}{2E} = \frac{\pi}{2} dp_t^2 dy_H \frac{d\varphi}{2\pi}. \quad (23)$$

Also, in the equation (20),  $\mathcal{M}$  is the matrix element of the  $g^*(k_1) + g^*(k_2) \rightarrow H(p)$  sub-process, given as (see the Appendix VII B):

$$|\mathcal{M}|^2 = \frac{\alpha_S^2(\mu^2)}{288\pi^2} \frac{G_F}{\sqrt{2}} \tau^2 |D(\tau)|^2 (m_H^2 + p_t^2)^2 \cos^2 \varphi. \quad (24)$$

In a high-energy inelastic collision at the LHC, one can consider the following kinematics for the center-of-mass frame

$$p_i = \frac{\sqrt{s}}{2} (1, 0, 0, \pm 1),$$

$$\mathbf{k}_i = x_i \mathbf{P}_i + \mathbf{k}_{i,\perp}, \quad \mathbf{k}_{i,\perp}^2 = -k_{i,t}^2, \quad i = 1, 2, \quad (25)$$

and express the law of the transverse momentum conservation for the  $g^*(k_1) + g^*(k_2) \rightarrow H(p)$  sub-process as:

$$\mathbf{k}_{1,\perp} + \mathbf{k}_{2,\perp} = \mathbf{p}_\perp, \quad (26)$$

with  $\mathbf{p}_\perp^2 = -p_t^2$  as the transverse momentum of the produced Higgs boson. Also, it is possible to write the longitudinal fractions  $x_i$  in terms of the transverse mass of the Higgs boson,  $m_{H,t}^2 \equiv m_H^2 + p_t^2$ , its rapidity and the parameter  $s$ ,

$$\begin{aligned} x_1 &= \frac{m_{H,t}}{\sqrt{s}} e^{+y_H}, \\ x_2 &= \frac{m_{H,t}}{\sqrt{s}} e^{-y_H}. \end{aligned} \quad (27)$$

Putting the above formulas together, we derive the master equation for the production of the Higgs bosons as:

$$\begin{aligned} \sigma_{P+P \rightarrow H+X} = & \frac{G_F}{\sqrt{2}} \int \frac{dk_{1,t}^2}{k_{1,t}^2} \frac{dk_{2,t}^2}{k_{2,t}^2} dy_H \frac{d\varphi}{2\pi} \cos^2 \varphi \\ & \times f_g(x_1, k_{1,t}^2, \mu_1^2) f_g(x_2, k_{2,t}^2, \mu_2^2) \\ & \times \frac{\alpha_S^2(\mu^2)}{144\pi} \frac{\tau^2 |D(\tau)|^2}{x_1 x_2 s m_H^2} (m_H^2 + p_t^2)^2. \end{aligned} \quad (28)$$

Benchmark	$\alpha_1$	$\alpha_2$	$\alpha_3$	$m_{h_1}$	$m_{h_2}$	$m_{h_3}$
A1	-0.047	-0.053	1.294	124.64	652.375	759.984
A2	-0.048	0.084	0.084	124.26	512.511	712.407
A3	0.078	0.297	0.364	124.27	582.895	650.531
A4	0.006	-0.276	0.188	125.86	466.439	568.059
A5	0.062	-0.436	0.808	125.21	303.545	582.496
A6	-0.210	0.358	0.056	124.92	181.032	188.82
A7	-0.205	0.403	0.057	125.01	175.45	178.52

TABLE I. Benchmark points A1 – A7. Masses are given in GeV and  $\alpha$  are the mixing angles [2].

To determine the density functions of the incoming gluons,  $f_g(x_i, k_{i,t}^2, \mu^2)$ , we utilize the KMR formalism,

$$f_g(x, k_t^2, \mu^2) = T_g(k_t^2, \mu^2) \frac{\alpha_S(k_t^2)}{2\pi} \int_x^{z_{max}} dz \times [P_{gq}^{(LO)}(z) \sum_q \frac{x}{z} q\left(\frac{x}{z}, k_t^2\right) + P_{gg}^{(LO)}(z) \frac{x}{z} g\left(\frac{x}{z}, k_t^2\right)]. \quad (29)$$

$z_{max} = \mu/(\mu + k_t)$  is a visualization of the angular ordering constraint, as a consequence of the color coherence effect of successive gluonic emissions [51].  $T_a(k_t^2, \mu^2)$  is the probability of survival, which limits the parton emissions between the scales  $k_t$  and  $\mu$ . It factors over the virtual contributions from the gluonic LO DGLAP equation and can be defined as:

$$T_g(k_t^2, \mu^2) = \exp\left[-\int_{k_t^2}^{\mu^2} \frac{\alpha_S(k^2)}{2\pi} \frac{dk^2}{k^2} \int_0^{z_{max}} dz \times \left(P_{gg}^{(LO)}(z) + n_f P_{gq}^{(LO)}(z)\right)\right], \quad (30)$$

with  $n_f$  being the number of involving quark flavors.  $P_{ab}^{(LO)}(z)$  are the LO splitting functions, parameterizing the probability of a parton with the longitudinal momentum fraction  $x$  to be emitted from a parent parton with the fraction  $x'$ , with  $z = x/x'$ , [46, 52].

In the following section, we will introduce some of the numerical methods that have been used in the calculation of the master equation (28), to predict the total cross-section of the production of the Higgs bosons of the cSMCS, with the lightest being the SM-like Higgs boson.

#### IV. NUMERICAL ANALYSIS

We use the UPDF of KMR, equation (29), to numerically solve the master equation (28), utilizing the VEGAS algorithm in Monte-Carlo integration, [53]. The required PDF for the preparation of these UPDF are provided in the form of phenomenological libraries, e.g. the MMHT2014 libraries, the reference [54], where the single-scaled solutions of the DGLAP evolution equations have been fitted with experimental data of the  $F_2$  structure

function from e-p deep inelastic scattering data. In addition, we chose the hard-scale of the UPDF as the transverse mass of the produced Higgs boson, i.e.

$$\mu = (m_H^2 + p_t^2)^{1/2}. \quad (31)$$

However, one should note that the upper and the lower boundaries on the transverse momentum integrations in the equation (28) are respectively  $\infty$  and zero. Nevertheless, since the KMR UPDF rapidly converge to zero in the  $k_t > \mu$  domain, it is safe to introduce an upper bound for these integrations, say

$$k_{t,max} = \mu_{max} \equiv 4(m_H^2 + p_{t,max}^2)^{1/2}. \quad (32)$$

Further domain have no contribution into our results. On the other hand, it is important to note that the UPDF of the  $k_t$ -factorization are being defined only in the QCD perturbative region, i.e. for  $k_t > \mu_0$  with  $\mu_0 = 1$  GeV, as the minimum scale for which the DGLAP evolution of the integrated PDF is valid. We have to define our treatment with these distribution functions in the non-perturbative region,  $k_t < \mu_0$ . A natural choice to by-pass this obstacle is to fulfill the requirement that

$$\lim_{k_{i,t}^2 \rightarrow 0} f_g(x_i, k_{i,t}^2, \mu^2) \sim k_{i,t}^2.$$

So, for the non-perturbative region, we choose

$$f_g(x_i, k_{i,t}^2 < \mu_0^2, \mu^2) = \frac{k_{i,t}^2}{\mu_0^2} x_i g(x_i, \mu_0^2) T_g(\mu_0^2, \mu^2). \quad (33)$$

Also, we set the boundaries of the rapidity integration in accordance with the specifications of the detectors of any given experimental report (i.e.  $|y_H| < 2.5$  for the CMS report [47] and  $|y_H| < 2.4$  for ATLAS reports [48, 49], excluding the  $1.37 < |y_H| < 1.52$  region for the later). Otherwise, we choose to integrate over the  $|y_H| < 10$  domain. According to the equation (27), and the  $0 < x_i < 1$  constraint, further rapidity domain will have no influence on our result.

At this point, we must mention that while calculating the total production rate of the SM Higgs boson in the collinear approximation, the higher order QCD corrections to the LO  $g^* + g^* \rightarrow H$  sub-process are significant. These correction are either kinematic in nature (e.g. corrections from the box and pentagon quark loops, see the

figure 1, parts (b) and (c)) or arise from real parton emissions or virtual loop corrections. It is however customary to compensate for these neglected contributions by the means of introducing an additional factor into the main calculations, called the K-factor, which is conventionally defined as the ratio of the corrected results to the LO results. It has been suggested that introducing a K-factor as

$$K(g^* + g^* \rightarrow H) \sim \exp\left(C_A \frac{\pi\alpha_S(\mu_c^2)}{2}\right), \quad (34)$$

with  $C_A = 3$  and  $\mu_c = (m_H p_t^2)^{1/3}$  can absorb the main part of these higher order corrections, [15].

Finally, we are ready to calculate the cross-section of the production of the SM and the cSMCS Higgs bosons, using the master equation (28) in the  $k_t$ -factorization framework. To switch from the SM to the cSMCS, we simply justify the mass of the Higgs boson, in accordance to the benchmarks of the cSMCS, the table I, and replace the SM Higgs-quark-quark coupling constant, from  $m_f/v$  with its cSMCS counterpart, i.e.  $R_{i1}m_f/v$ .

## V. RESULTS AND DISCUSSIONS

Here, we present our numerical result. Before discussing our cSMCS predictions, it is necessary to prove that our framework can in fact produce reliable results. Hence, the figure 2 presents the reader with the differential cross-section of the production of the SM Higgs boson ( $d\sigma_H/dp_t$ ) versus the transverse momentum of the produced particle ( $p_t$ ). Parts (a) and (b) illustrate our results for the center-of-mass energy  $E_{CM} = 8$  TeV and the rapidity regions  $|y_H| < 2.4$  and  $|y_H| < 2.5$ , respectively. The main results are being presented by solid black curves while the blue stripped patterns mark the uncertainty bounds (which are determined by manipulating the hard-scale  $\mu$  by a factor of 2). Part (c) shows the same set of calculations in the center-of-mass energy  $E_{CM} = 13$  TeV and rapidity region  $|y_H| < 2.4$  (excluding the  $1.37 < |y_H| < 1.52$  region). The data points are the measurements of the CMS and the ATLAS collaborations, references [47–49]. A similar comparison is presented in the figure 3, regarding the rapidity contribution of the Higgs boson production. i.e.  $d\sigma_H/dy_H$  versus  $y_H$ . It appears that our framework, at least within its uncertainty bounds, can produce an acceptable approximation for the production of the Higgs particles in the high-energy QCD events.

Figure 4, illustrates our predictions for the production of Higgs bosons in  $E_{CM} = 14$  TeV, where the differential cross-section computations are shown as functions of the Higgs  $p_t$ . Part (a) depicts the general behavior of this production rate, exclusively within the SM. Part (b) outlines an interesting comparison between our calculations and the similar results from NLL+LO (next-to-leading logarithmic re-summation plus LO calculations) and NLL+NLO (next-to-leading logarithmic

re-summation plus NLO calculations) frameworks in the collinear factorization, from the reference [17]. The collinear results show a slightly higher peak, compared to the KMR framework. Otherwise, the general behavior of these frameworks are identical. One should note that the collinear results each have an uncertainty bound, expectantly smaller (and therefore, inside) our uncertainty region. In the part (c), we demonstrate the differential cross-section of the production of the SM-like Higgs boson from the cSMCS. The curves A1 through A7 correspond to the cSMCS benchmarks, the table I. These computations are presented with respect to the SM uncertainty bounds. Also, the figure 5 presents a similar comparison regarding the  $y_H$  contribution of the Higgs boson production for the SM and the cSMCS.

Furthermore, we have calculated the total rate of production of the SM Higgs particles ( $\sigma_H$ ) as a function of the center-of-mass energy of the hadronic collision ( $E_{CM}$ ), the figure 6, and compared the results with the existing experimental data, see the references [47–49]. The notion of the diagram is as before, and again, the predictions seem to be acceptable. Another interesting evaluation would be to compute the mass distribution of the Higgs boson production, presented as the figure 7. The peculiar bump in the cross-section is originated from the imaginary part of  $D(\tau)$ , the equation (41), which becomes non-zero at  $m_H = 2m_t$ .

At this point, after investigating the relative of our framework in describing the SM Higgs production via inelastic hadronic collisions at the LHC, it is time to go forward and present our predictions regarding the expected rate of the production of the cSMCS Higgs particles in the high-energy QCD events. Therefore, the figures 8 and 9, present the reader with a comparison of the differential cross-sections for the production of these particles, labeled as A1 through A7, in accordance with their physical specifications (given in the table I), as the benchmarks of the cSMCS. The calculations have been performed using the UPDF of KMR, with  $E_{CM} = 14$  TeV, illustrating the transverse momentum and rapidity distributions of these differential cross-sections. Parts (a), (b) and (c) correspond to the first (SM-like), second and the third cSMCS Higgs boson, respectively. It is apparent that the behavior of these predictions is rather diverse, covering different kinematic regions. Nevertheless, these computations, presented in the figures 8 and 9, are a set of reliable simulations for the Higgs signal within the cSMCS and will serve particularly useful in the on-going experimental research regarding light and heavy Higgs bosons at the LHC.

## VI. CONCLUSIONS

Throughout the present work, we have calculated the production rates for the Higgs bosons of the SM and the cSMCS, using an effective LO partonic matrix element and the UPDF of the KMR formalism. The calculations

for the SM Higgs boson have been compared with the existing experimental data of the CMS and the ATLAS collaborations, showing that our computations, within the given uncertainty bounds, present an acceptable platform to describe the dynamics of the Higgs production at the LHC, and argued that introducing higher-order corrections into our framework is expected to increase the precision of these calculations. Afterwards, we have presented our predictions, regarding the distribution of the transverse momentum and the rapidity of the SM-like and heavy Higgs boson production, from the cSMCS via inelastic hadronic collisions at the LHC, providing a reliable base-line for further experimental research. At the moment, there are no experimental evidence that support the existence of such heavy scalar bosons. Yet, it is widely believed that such particles are the necessary parts of a model that can fully describe the dynamics of fundamental particles. Detecting the second Higgs boson, if happen, will open the doors for further exploration of these ideas. In that case, the predictions that are presented within this work will provide some clues regarding the dynamics of the next discovery.

## ACKNOWLEDGMENTS

The authors sincerely thank Professor M. Modarres and Professor M. Krawczyk for reviewing this work and for instructive comments.

*ND* is supported in part by the National Science Center, Poland, the HARMONIA project under contract UMO-2015/18/M/ST2/00518.

*MRM* acknowledges R. Aminzadeh-Nik for his valuable discussions and comments.

## VII. APPENDIX

### A. Extremum Conditions

The extremum conditions lead to the following constraints,

$$-m_{11}^2 + v^2\lambda_1 + 2\sqrt{2}w_1\kappa_4 + \Lambda w^2 = 0, \quad (35)$$

$$w_1(-\mu_1^2 + v^2\Lambda + 2w^2\lambda_s) + \sqrt{2}[3(w_1^2 - w_2^2)\kappa_2 + (3w_1^2 + w_2^2)\kappa_3] + v^2\sqrt{2}\kappa_4 = 0, \quad (36)$$

$$w_2[-\mu_2^2 + v^2\Lambda + 2w^2\lambda_s + 2\sqrt{2}w_1(-3\kappa_2 + \kappa_3)] = 0, \quad (37)$$

with the parameters  $\mu_1^2$  and  $\mu_2^2$  defined as

$$\mu_1^2 = m_s^2 + 2m_4^2, \quad \mu_2^2 = m_s^2 - 2m_4^2.$$

Here we concentrate on non vanishing  $v, w_1$  and  $w_2$ , allowing for a vacuum which violate CP.

### B. Matrix Element

Deriving an analytic expression for  $\mathcal{M}$  is mathematically involved, specially with non-negligible transverse momenta for the incoming gluons. Using the Feynman rules for the diagram (a) of the figure 1 (and its permutation), one can readily write the corresponding matrix element as:

$$\begin{aligned} \mathcal{M}(g^*(k_1) + g^*(k_2) \rightarrow H(p)) &= 2\pi\alpha_S(\mu^2) \int_0^\infty \frac{d^4q}{(2\pi)^4} \\ &\times m_t \left( \frac{G_F}{\sqrt{2}} \right)^{1/2} \text{Tr} \left\{ \frac{\gamma \cdot (q + k_2) + m_t}{(q + k_2)^2 - m_t^2} \right. \\ &\times [\gamma_\mu \epsilon_a^\mu(\lambda_1, \mathbf{k}_1) t^a] \frac{\gamma \cdot (q) + m_t}{q^2 - m_t^2} [\gamma_\nu \epsilon_b^\nu(\lambda_2, \mathbf{k}_2) t^b] \\ &\times \left. \frac{\gamma \cdot (q - k_1) + m_t}{(q - k_1)^2 - m_t^2} + [k_1 \leftrightarrow k_2] \right\}. \end{aligned} \quad (38)$$

In the equation (38),  $\alpha_S$  and  $G_F$  are respectively the running coupling constant of the strong interaction and the Fermi's constant.  $q$  is the 4-momenta of the exchanged particle in the top-quark loop.  $\epsilon_a^\mu(\lambda_i, \mathbf{k}_i)$  are the polarization functions of the incoming gluons, relative to their spin state ( $\lambda_i$ ), their momenta and their color state (denoted by the color index  $a$ ) and  $t^a$ , the Gell-Mann matrices which are the generators of the  $SU(3)$  gauge group. To calculate  $|\mathcal{M}|^2$ , one have to multiply the expression (38) by its complex conjugate, do the traces and perform the integration. Additionally, since the incoming gluons are virtual, one have to take into account the so-called non-sense polarization (see the references [44, 55]) through the following identity:

$$\sum_\lambda \epsilon^\mu(\lambda, \mathbf{k}_i) \epsilon^{*\nu}(\lambda, \mathbf{k}_i) = \frac{k_{i,t}^\mu k_{i,t}^\nu}{\mathbf{k}_{i,t}^2}. \quad (39)$$

Hence, after rather lengthy calculations, one obtains:

$$|\mathcal{M}|^2 = \frac{\alpha_S^2(\mu^2)}{288\pi^2} \frac{G_F}{\sqrt{2}} \tau^2 |D(\tau)|^2 (m_H^2 + p_t^2)^2 \cos^2\varphi, \quad (40)$$

where  $\tau = 4m_t^2/m_H^2$  and

$$\begin{aligned} D(\tau < 1) &= \frac{3}{2} \left[ 1 + \frac{1-\tau}{2} \left( \ln \frac{1+\sqrt{1-\tau}}{1-\sqrt{1-\tau}} - i\pi \right)^2 \right], \\ D(\tau \geq 1) &= \frac{3}{2} \left[ 1 + (1-\tau) \arcsin^2 \left( \frac{1}{\sqrt{\tau}} \right) \right]. \end{aligned} \quad (41)$$

It is easy to confirm that at the limit of large  $m_t$ , i.e. as  $\tau \rightarrow \infty$ ,

$$\lim_{\tau \rightarrow \infty} \tau D(\tau) = 1 + \mathcal{O}\left(\frac{1}{\tau}\right). \quad (42)$$

Afterwards, neglecting the transverse momentum of the produced boson,  $p_t \rightarrow 0$ , the equation (24) returns to its conventional form in the collinear approximation, [56].

- 
- [1] N. Darvishi, arXiv:1608.02820 [hep-ph].
  - [2] N. Darvishi and M. Krawczyk, arXiv:1603.00598 [hep-ph].
  - [3] M. Krawczyk, N. Darvishi and D. Sokolowska, Acta Phys. Polon. B **47** (2016) 183 doi:10.5506/APhysPolB.47.183 [arXiv:1512.06437 [hep-ph]].
  - [4] S. Profumo, M. J. Ramsey-Musolf and G. Shaughnessy, JHEP **0708** (2007) 010 [arXiv:0705.2425 [hep-ph]].
  - [5] G. C. Branco, P. A. Parada and M. N. Rebelo, hep-ph/0307119.
  - [6] E. Gabrielli, M. Heikinheimo, K. Kannike, A. Racioppi, M. Raidal and C. Spethmann, Phys. Rev. D **89** (2014) 1, 015017 doi:10.1103/PhysRevD.89.015017 [arXiv:1309.6632 [hep-ph]].
  - [7] J. Kozaczuk, JHEP **1510** (2015) 135 doi:10.1007/JHEP10(2015)135 [arXiv:1506.04741 [hep-ph]].
  - [8] M. Jiang, L. Bian, W. Huang and J. Shu, Phys. Rev. D **93**, no. 6, 065032 (2016) doi:10.1103/PhysRevD.93.065032 [arXiv:1502.07574 [hep-ph]].
  - [9] L. Alexander-Nunneley and A. Pilaftsis, JHEP **1009** (2010) 021 doi:10.1007/JHEP09(2010)021 [arXiv:1006.5916 [hep-ph]].
  - [10] V. Barger, P. Langacker, M. McCaskey, M. Ramsey-Musolf and G. Shaughnessy, Phys. Rev. D **79** (2009) 015018 doi:10.1103/PhysRevD.79.015018 [arXiv:0811.0393 [hep-ph]].
  - [11] J. R. Espinosa, B. Gripaios, T. Konstandin and F. Riva, JCAP **1201** (2012) 012 [arXiv:1110.2876 [hep-ph]].
  - [12] R. Costa, A. P. Morais, M. O. P. Sampaio and R. Santos, Phys. Rev. D **92** (2015) 025024 [arXiv:1411.4048 [hep-ph]].
  - [13] O. Lebedev, Phys. Lett. B **697** (2011) 58 [arXiv:1011.2630 [hep-ph]].
  - [14] C. Bonilla, D. Sokolowska, N. Darvishi, J. L. Diaz-Cruz and M. Krawczyk, arXiv:1412.8730 [hep-ph].
  - [15] G. Watt, A.D. Martin and M.G. Ryskin, Phys.Rev.D **70** (2004) 014012.
  - [16] A.V. Lipatov, N.P. Zotov, Eur. Phys. J. C **44** (2005) 559-566.
  - [17] M. Grazzini, CERN-PH-TH/2004-107, arXiv:hep-ph/0406156.
  - [18] X. Chen, J. Cruz-Martinez, T. Gehrmann, E.W.N. Glover, M. Jaquier, IPPP/16/73, ZU-TH 29/16, FR-PHENO-2016-014, arXiv:1607.08817.
  - [19] G. Ferrera, J. Pires, MPP-2016-152, TIF-UNIMI-2016-7, arXiv:1609.01691.
  - [20] P. F. Monni, E. Re, P. Torrielli, Phys. Rev. Lett. **116** (2016) 242001.
  - [21] D. de Florian, DESY 16-107, FR-PHENO-2016-007, ICAS 08/16, MITP/16-061, ZU-TH 20/16, arXiv:1606.09519.
  - [22] S. Liebler, H. Mantler, M. Wiesemann, DESY 16-146, KA-TP-24-2016, ZU-TH 27/16, arXiv:1608.02949.
  - [23] F. Caola, S. Forte, S. Marzani, C. Muselli, G. Vita, JHEP **08** (2016) 150.
  - [24] V.N. Gribov and L.N. Lipatov, Yad. Fiz., **15** (1972) 781..
  - [25] L.N. Lipatov, Sov.J.Nucl.Phys., **20** (1975) 94.
  - [26] G. Altarelli and G. Parisi, Nucl.Phys.B, **126** (1977) 298.
  - [27] Y.L. Dokshitzer, Sov.Phys.JETP, **46** (1977) 641.
  - [28] M.A. Kimber, A.D. Martin and M.G. Ryskin, Phys.Rev.D, **63** (2001) 114027.
  - [29] A.D. Martin, M.G. Ryskin, G. Watt, Eur.Phys.J.C, **66** (2010) 163.
  - [30] M.A. Kimber, J. Kwiecinski, A.D. Martin, A.M. Stasto, Phys.Rev.D **62**, (2000) 094006.
  - [31] M.A. Kimber, Unintegrated Parton Distributions, Ph.D. Thesis, University of Durham, U.K. (2001).
  - [32] M. Ciafaloni, Nucl.Phys.B, **296** (1988) 49.
  - [33] S. Catani, F. Fiorani, and G. Marchesini, Phys.Lett.B, **234** (1990) 339.
  - [34] S. Catani, F. Fiorani, and G. Marchesini, Nucl.Phys.B, **336** (1990) 18.
  - [35] M. G. Marchesini, Proceedings of the Workshop QCD at 200 TeV Erice, Italy, edited by L. Cifarelli and Yu.L. Dokshitzer, Plenum, New York (1992) 183.
  - [36] G. Marchesini, Nucl.Phys.B, **445** (1995) 49.
  - [37] V.S. Fadin, E.A. Kuraev and L.N. Lipatov, Phys. Lett. B, **60** (1975) 50.
  - [38] L.N. Lipatov, Sov.J.Nucl.Phys., **23** (1976) 642.
  - [39] E.A. Kuraev, L.N. Lipatov and V.S. Fadin, Sov. Phys. JETP, **44** (1976) 45.
  - [40] E.A. Kuraev, L.N. Lipatov and V.S. Fadin, Sov. Phys. JETP, **45** (1977) 199.
  - [41] Ya.Ya. Balitsky and L.N. Lipatov, Sov.J.Nucl.Phys., **28** (1978) 822.
  - [42] M. Modarres, H. Hosseinkhani, N. Olanj and M.R. Masouminia, Eur. Phys. J. C **75** (2015) 556.
  - [43] M. Modarres, M.R. Masouminia, H. Hosseinkhani, and N. Olanj, Nucl. Phys. A **945**(2016)168185.
  - [44] M. Modarres, M.R. Masouminia, R. Aminzadeh Nik, H. Hosseinkhani, N. Olanj, Phys. Rev. D **94** (2016) 074035.
  - [45] M. Modarres, M.R. Masouminia, R. Aminzadeh Nik, arXiv:1610.02635.
  - [46] M. Modarres, M.R. Masouminia, arXiv:1610.02777.
  - [47] V. Khachatryan et al. [CMS Collaboration], Eur. Phys. J. C **76** (2016) 13.
  - [48] G. Aad et al. [ATLAS Collaboration], JHEP **1409** (2014) 112.
  - [49] ATLAS Collaboration, ATLAS-CONF-2016-067.
  - [50] S. Catani, M. Ciafaloni, F. Hautmann, Nucl. Phys. B **366**, 135 (1991).
  - [51] M.A. Kimber, A.D. Martin and M.G. Ryskin, Eur. Phys. J. C **12** (2000) 655.
  - [52] W. Furmanski, R. Petronzio, Phys. Lett. B **97**, 437 (1980).
  - [53] G. P. Lepage, J. Comput. Phys. **27** (1978) 192.
  - [54] L. A. Harland-Lang, A. D. Martin, P. Motylinski, R.S. Thorne, Eur.Phys.J.C **75** (2015) 204.
  - [55] M. Deak, Transversal momentum of the electroweak gauge boson and forward jets in high energy factorisation at the LHC, Ph.D. Thesis, University of Hamburg, Germany, 2009.
  - [56] F. Hautmann, Phys. Lett. B **535**, 159 (2002).



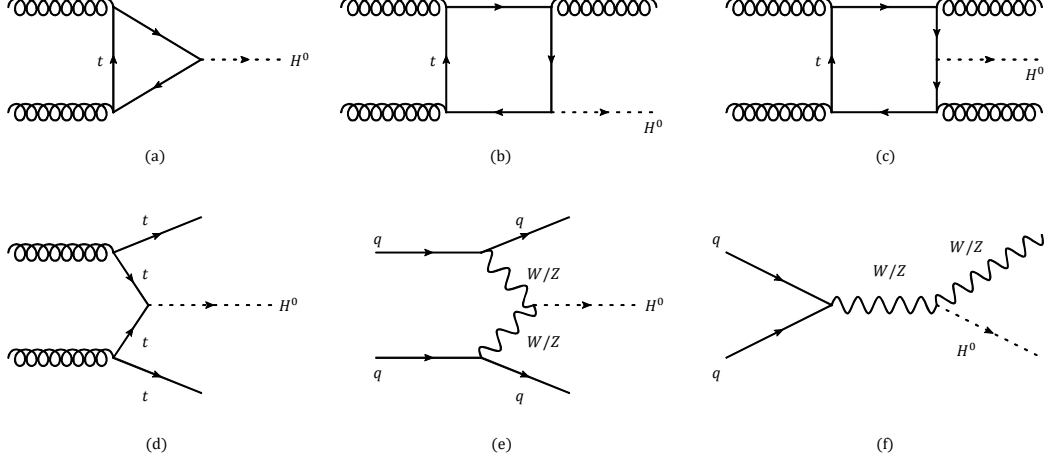


FIG. 1. The main contributing sub-processes in the total cross-section of the production of the Higgs bosons in the LHC. Sub-processes (a), (b) and (c) illustrate the gluon-gluon fusion process, respectively in the triangular, box and pentagon top-quark loops. The sub-process (d) shows the  $tt$ -fusion while (e) and (f) are the  $W/Z$  Bremsstrahlung sub-processes.

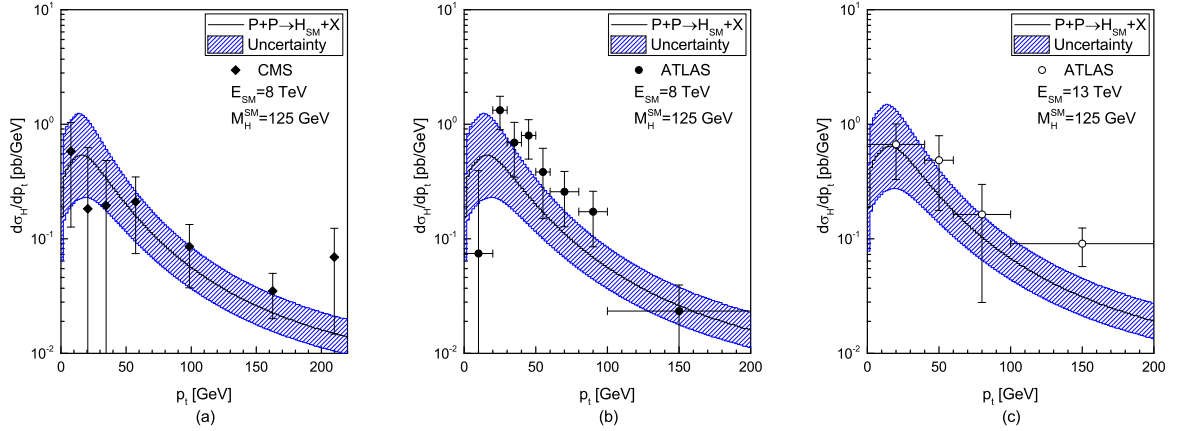


Figure 2

FIG. 2. Differential cross-section of the production of the SM Higgs boson as a function of the transverse momentum of the produced particle. The calculations have been performed for the center-of-mass energies  $E_{cm} = 8$  TeV and 13 TeV. The black solid curves illustrate the main out-puts while the blue stripped patterns show the uncertainty bound for the results. The uncertainty bounds are determined via manipulating the hard-scale  $\mu$  by a factor of 2. The results have been compared with the experimental data from the CMS and the ATLAS collaborations, [47–49]. To prepare the KMR UPDF, we have utilized the PDF of MMHT2014.

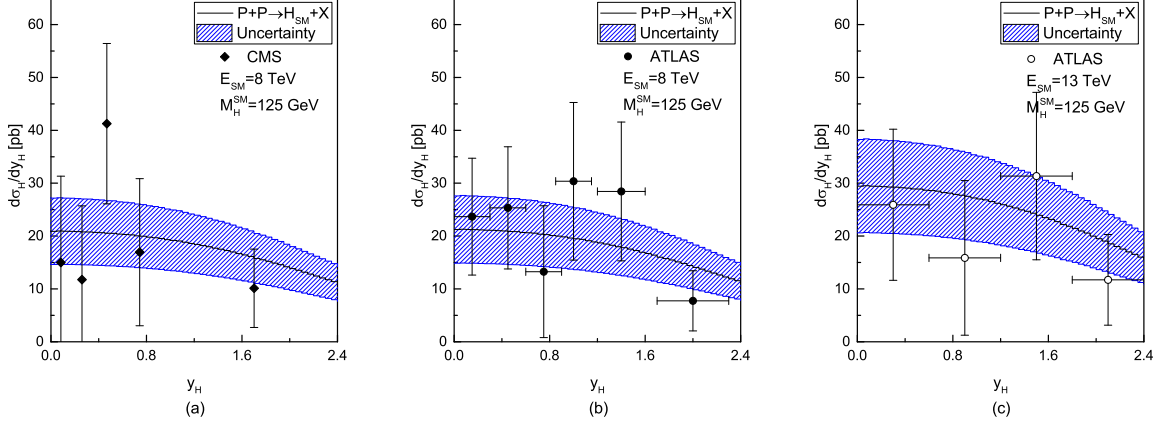


Figure 3

FIG. 3. Differential cross-section of the production of the SM Higgs boson as a function of the rapidity of the produced particle. The calculations have been performed for the center-of-mass energies  $E_{cm} = 8$  TeV and 13 TeV. The notion of the diagram is as in the figure 1.

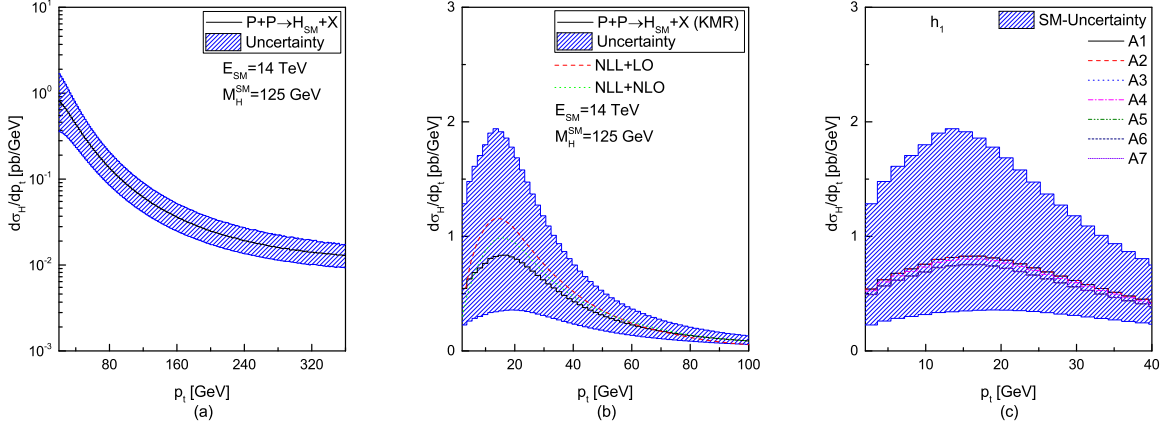


Figure 4

FIG. 4. Differential cross-section of the production of the Higgs boson as a function of the transverse momentum of the produced particle with  $E_{CM} = 14$  TeV. Part (a) illustrates the main results and the corresponding uncertainty bounds for the SM higgs boson. Part (b) presents a comparison between our results (the solid black curve and its blue strip-patterned uncertainty bounds) and the results of similar calculations within the collinear framework, i.e. the NLL+LO (red dashed curve) and the NLL+NLO (dotted green curve). The collinear results are from the reference [17]. Part (c) presents the benchmark predictions of the cSMCS for the lightest Higgs boson (SM-like Higgs boson). The calculations for the benchmarks A1 through A7 have been performed with respect to their physical specifications, see table I also the section 6.4 of the reference [2].

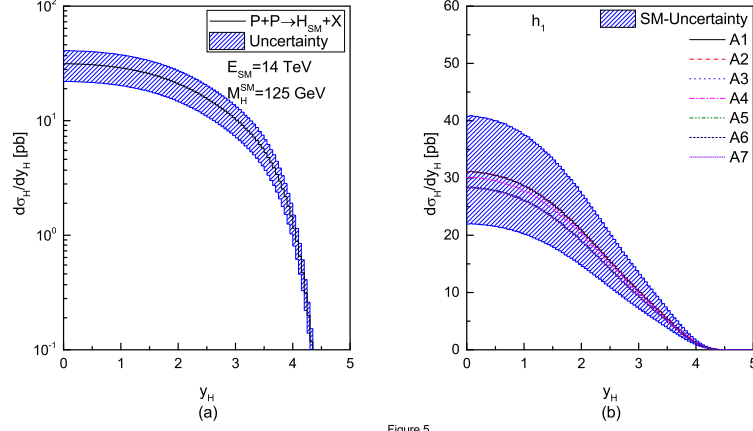


Figure 5

FIG. 5. Differential cross-section of the production of the Higgs boson as a function of the rapidity of the produced particle with  $E_{CM} = 14$  TeV. The notion of the diagrams is as in the parts (a) and (c) of the figure 4.

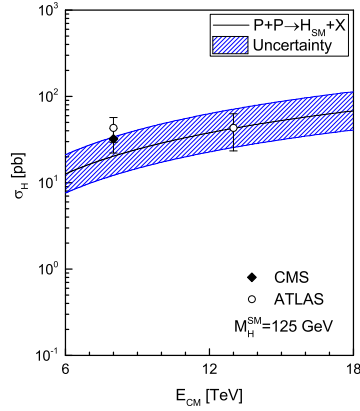


Figure 6

FIG. 6. Inclusive total cross-section of the production of the Higgs boson as a function of the central-mass energy of the inelastic proton-proton collision, at the LHC. The solid black curve illustrates the main results while the uncertainty bounds (blue stripped pattern) have been produced via manipulating the hard-scale of the UPDF,  $\mu$ , by a factor of 2. The experimental data are from the CMS (black diamonds) and the ATLAS (white circles) collaborations, [47–49].

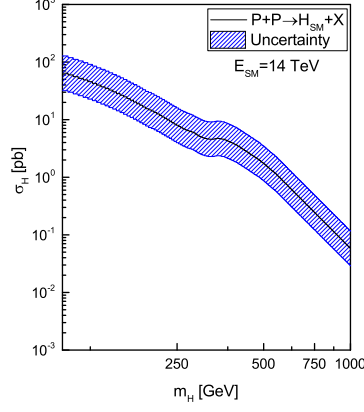


Figure 7

FIG. 7. Inclusive total cross-section of the production of the Higgs bosons as a function of the mass of the produced particle. The notion of the diagram is as in the figure 6.

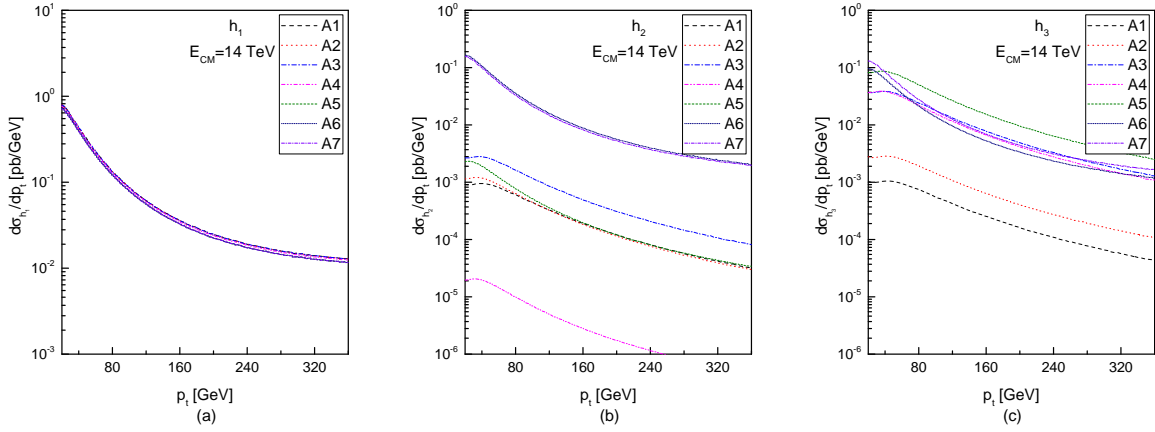


Figure 8

FIG. 8. Differential cross-section of the production of the sSMCS Higgs bosons as a function of the transverse momentum of the produced particles with  $E_{CM} = 14$  TeV. Parts (a), (b) and (c) present the benchmark predictions of the cSMCS Higgs bosons,  $h_1$ ,  $h_2$  and  $h_3$  ( $m_{h_1} < m_{h_2} < m_{h_3}$ ), in accordance with the benchmarks given in the table I (and also in the reference [2]), marked by A1 through A7.

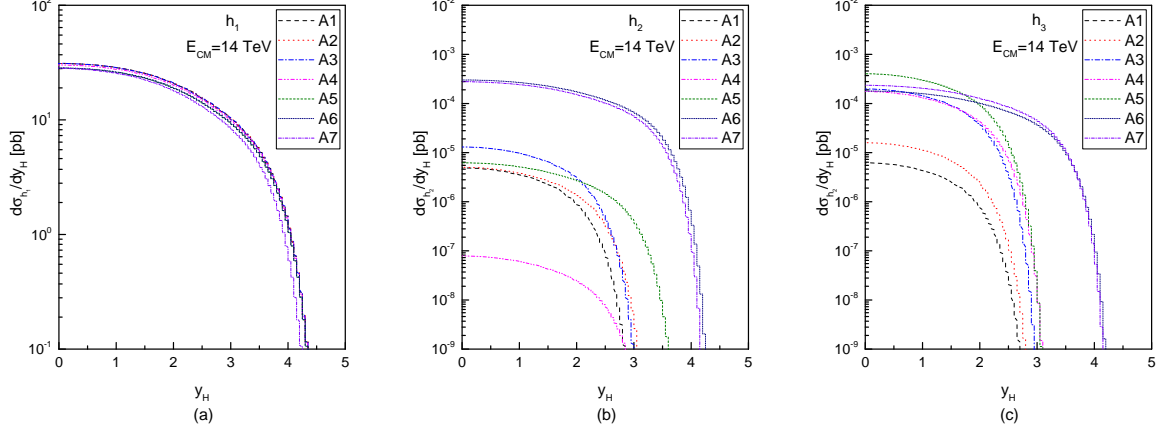


Figure 9

FIG. 9. Differential cross-section of the production of the sSMCS Higgs bosons as a function of the rapidity of the produced particles with  $E_{CM} = 14$  TeV. The notion of the diagrams is as in the figure 8.